 doi:10.20944/preprints202103.0772.v1

Article

Wind-Water experimental analysis of small SC-Darrieus turbine: an approach for energy production in urban systems

Ahmed Gharib-Yosry[1,2], Eduardo Blanco-Marigorta[1], Aitor Fernández-Jiménez[3], Rodolfo Espina-Valdés[3], Eduardo Álvarez-Álvarez[3]*.

[1] Energy Department, University of Oviedo, C/ Wifredo Ricart s/n, Gijon, Spain; eblanco@uniovi.es
[2] Mechanical Power Department, Faculty of Engineering, Port Said University, Egypt; uo248745@uniovi.es
[3] Hydraulic R&D Group, EP Mieres, University of Oviedo, Gonzalo Gutiérrez Quirós, 33600, Mieres, Spain; fernandezaitor.fuo@uniovi.es, espinarodolfo@uniovi.es
* Correspondence: edualvarez@uniovi.es

Abstract: Smart cities will have a strong impact on the future of renewable energies as terms like sustainability and energy saving will be more common. In this sense, both of wind and hydrokinetic compact-size turbines, can play an important role in urban communities by providing energy to nearby consumption points in an environmentally suitable way. This work presents the experimental evaluation for a vertical-axis turbine Darrieus type, operating in an open-field wind tunnel and a confined water channel. Power and characteristic curves have been obtained for all test conditions, also the effect of turbine blockage has been evaluated under blockage values ranging from 6.8% to 35%. The peak power coefficient for the confined flow condition reached a value of 0.31 which is 1.5 times higher than the peak one for the experimental open field condition at the same Reynolds number and a blockage of 20%. Finally, two blockage correction equations have been applied to the water channel tests, which gave values quite similar to the results obtained from the wind tunnel.

Keywords: Sustainability; Urban energy systems; wind turbine; hydrokinetic turbine; blockage.

1. Introduction

Significant progresses have been made at the energy sector to generate electricity from sustainable renewable resources, such as the improvement in solar panels performance [1] or the installation of offshore wind arrays [2]. Other low-carbon resources, such as the energy from flowing water currents, both marine and terrestrial, can become clean energy alternatives suitable for their use. Thus, future energy demands will be covered, reducing gas emissions to the atmosphere, and fighting against climate change.

In 2020, the outbreak of the pandemic caused by the COVID-19 tested the strength of the world's electricity system. During the first semester, coinciding with the hardest months of the disease and confinements, the world energy demand suffered a notable decrease of 5%, mainly due to the interruption of industrial activity [3]. However, the demand of renewable energy increased 1%, showing great resilience. Thus, the hypo-carbon energy sector has shown an extraordinary ability of adaptation to this new situation, participating more than a 18% of what it was expected in 2019. Different factors, such as their independence in the transport of resources (they are located where the resource is available) or their installation at isolated ubications, are the main reasons of this extraordinary resilience [4].

In this way, recent studies have estimated that green energy will grow up a 10% in 2021, 3% more than expected, because of the resumption of projects that were blocked by the pandemic. For this, more than hundred million dollars, mainly in Europe, United States, China and India, will be invested to build these facilities so that the zero-emissions goal can be reached by 2030 [5].

Preprints (www.preprints.org) | NOT PEER-REVIEWED | Posted: 31 March 2021 doi:10.20944/preprints202103.0772.v1

Part of this investment will be destinated to research and develop systems based on hydrokinetic turbines for it use at ocean and flowing currents. These systems will harness the great potential that exists in those locations which, in the case of marine currents, is worldwide estimated in 800 TWh/year [3]. In the case of flowing channels, only in Spain it has been estimated an energy potential of 840 MWh/year [6]. These resources are predictable over time and their energetic use can be compatible with other uses such as water supply [7], what gives them versality and flexibility.

Recently, and related with Smart Cities, some proposals based on microgeneration using turbines are being developed [8]. Thus, the proposed rotors of this work are based on the use of turbines with dual operating characteristics so these devices can work both with water and wind. This versatility gives them competitive advantages by reducing their cost and facilitating their manufacture since they do not require specific changes in their design to adapt to the working fluid. This is possible due to the use of lift-based rotors, the installation of permanent magnet generators and the development of much more efficient electronic control systems [9]. Thus, the structure and control elements are simplified, so that the visual impact and cost are minimized, making them very attractive to be installed in urban environments [10]. Figure 1 shows a dual proposal composed by hydrokinetic turbines and wind turbines using the same rotor design to harness both resources. In this case, the energy is used to supply electricity and other services to a city.

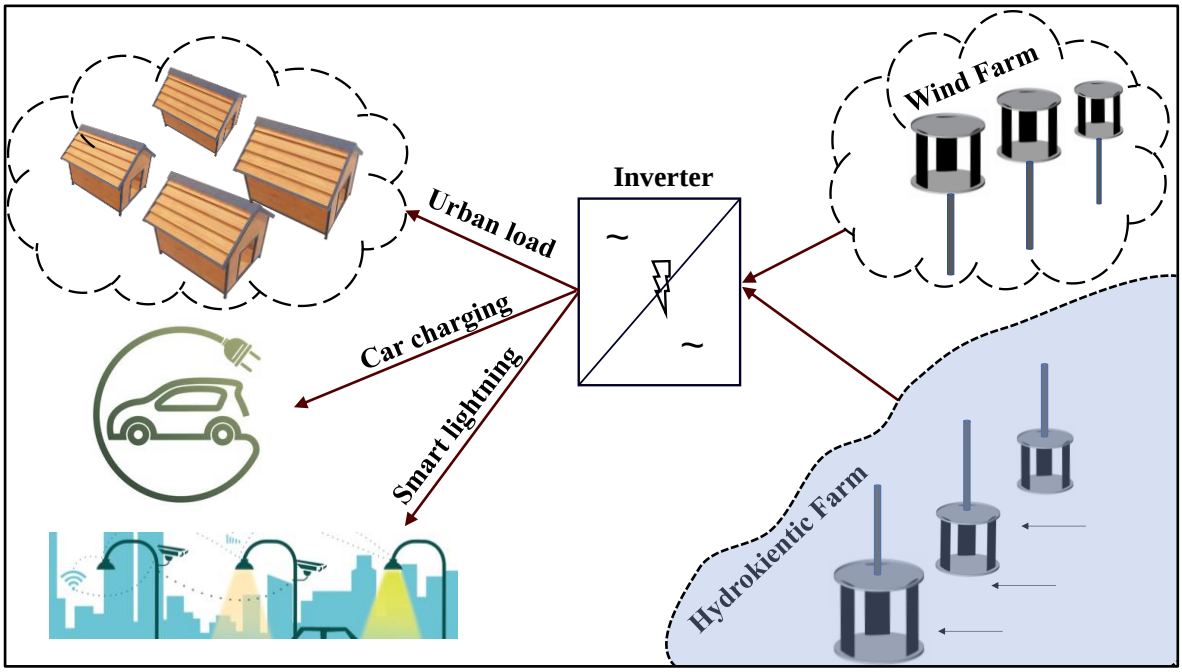

Figure 1. Energy production and utilization approach in urban system using hydrokinetic and wind turbines.

While the wind industry has reached a high degree of technological maturity, the use of hydrokinetic turbines is the most sustainable way to harness flowing water currents in free sheet conditions since they do not require diversion works or other infrastructures. These devices use the kinetic term of the current, not requiring the creation of height differences, so not only the installation requires less initial investment but also the environmental impact is minimized [11]. Thus, the power obtained by these turbines will mainly depend on the water velocity, together with the area swept by their blades, the fluid density, and the conversion efficiency of the equipment.

Hydrokinetic turbines can be classified into two large groups according to the direction of the flow and the axis of rotation: axial turbines (flow and parallel axis) and crossflow turbines (flow and perpendicular axis). Nowadays, crossflow turbines are the ones that generates more interest [12]. This is mainly because these rotors, although are not efficient as axial ones, they have a much simpler mechanical coupling system that reduces the construction costs and facilitates installation and maintenance activities [13]. One of

Preprints (www.preprints.org) | NOT PEER-REVIEWED | Posted: 31 March 2021 doi:10.20944/preprints202103.0772.v1

the most used crossflow rotor design is Darrieus type, being Squirrel Cage (SC), H and curved the main examples [14] (Figure 2). These designs base their design on aerodynamical profiles used at the wind industry [15].

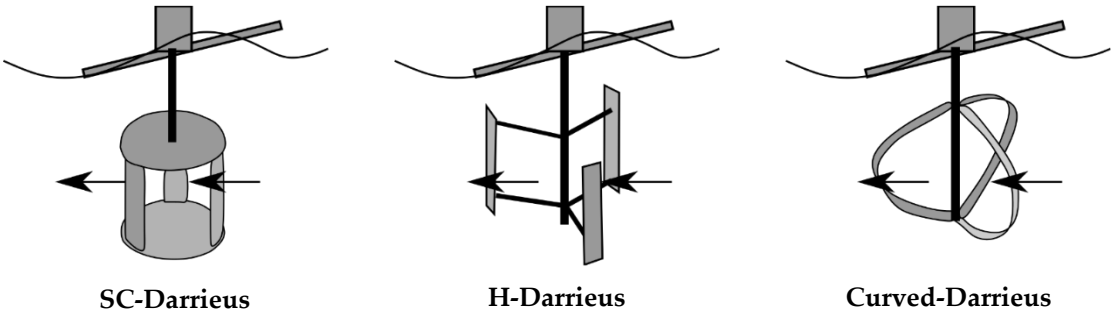

Figure 2. Different designs of Darrieus rotors

Crossflow rotors can be divided according to the axis position into horizontal and vertical axis turbines. Although horizontal turbines have been used mainly for shallow-water conditions [16], vertical rotors allow a greater use of the cross-sectional area of the water current when they are arranged in farms or arrays, allowing the production of energy under low-velocity conditions [17]. Also, because their dimensions rarely exceed 2 meters height and diameter, they have less effect on the environment or the river-maritime traffic [18].

The use of vertical axis water turbines under low-velocity and shallow water conditions is possible due to the appearance of blockage phenomenon. This phenomena is produced because of the presence of the rotor in the water stream and causes an increase in power and thrust compared with the flow behavior at open-field conditions [19]. Under these circumstances, three simultaneous phenomena appear: increase in the fluid velocity around the rotor, high pressure changes in produced wakes and the appearance of longitudinal pressure gradients associated to boundary layer conditions [20].

Until now, blockage has been studied from two different points of view: energetic use of the blockage effect and development of mathematical corrections to extrapolate their behavior to open-field conditions. In the first point of view, it is studied the design of devices, such as accelerator or deflectors, to induce blockage conditions into the water stream current [11]. In the second point of view, different numerical methodologies are developed to eliminate the effects of blockage that inherently appear in experimental tests and extrapolate that behavior to open-field conditions [21].

More specifically, most accelerators studies have tested different designs observing the increases in the extracted power for the same hydrodynamic conditions. Some examples are the results presented by [22] and [23]. In the case of blocking corrections, the development of numerical expressions to correct these effects are mainly based on the application of the simple actuator disc theory and the use of empirical coefficients. The results presented by [20], [24], [25] shows the value of the corrected open-field velocity from a theoretical energy study, while [21], [26] provide empirical correction coefficients based on laboratory tests. In both cases, these studies are approached from numerical models, based on Computational Fluid Dynamics (CFD) and experimental tests.

However, since the corrections of blockage effects are not yet sufficiently precise, other researching alternatives should be considered to address this issue. Accordingly, the study of blockage conditions is being approached by using two different devices: wind and water tunnel. Although the physical conditions are not the same since they are two different fluids, the way in which the turbine extracts energy is analogous, so results can be compared. Thus, the power characterization of the rotor under blockage conditions will be made at the water current flume while, at the wind tunnel, the turbine will be studied under open-field conditions. In this way, power parameters will be obtained such as the

Preprints (www.preprints.org) | NOT PEER-REVIEWED | Posted: 31 March 2021 doi:10.20944/preprints202103.0772.v1

power coefficient (Cp), the tip speed ratio (λ) and the conditions at the maximum power point (MPP).

Different authors have approached the study of blockage in crossflow turbines under confined and open-field conditions. These studies have been carried out using wind and water tunnels, sometimes even simultaneously. On the one hand, some confined flow studies such as the one carried out by Hossein et al [27], analyzed the effects of blockage and the position of the water free surface on the energy extracted by the rotor. It concludes that there is a clear relationship between both aspects since there is a change in the hydrodynamic operation of the acting forces. This study was approached using a high-speed camera and a torque meter. Also of interest is the work presented by Bachant et al [28] in which a comparison was made between Gorlov and Savonius rotors under blockage conditions. In this case, the study concludes that Gorlov turbines are more recommended when blockage coefficient is low (< 20%).

On the other hand, open-field studies, such as those carried out by Banerjee et al [29] and Consul et al [30], have analyzed how certain parameters such as solidity or wake appearance affect the power extraction. In the first case, the power stage of a tidal turbine at a wide water tunnel was studied, measuring wake effects when current velocity was increased. It was observed that there is a threshold beyond which wake effects which negatively affects the power extraction. In the second work, carried out in a wind tunnel and complemented with a numerical model, it was concluded that when the blockage coefficient increases, there is also an increase of the rotation speed that favors energy extraction.

Finally, some studies have been made using both wind and water tunnel. For example, the studies presented by [31] and [32] carried out tests with wind turbines, obtaining the power stage behavior at wind tunnel and analyzing, using PIV (Particle Image Velocimetry) techniques, the stall appearances on blades. Hence, it was possible to quantify the detachment effect so the blade design could be adjusted. Other studies such as the one carried by [33] or [34] tested axial turbines in wind and water tunnels to study in which fluid the chosen designs where more suitable. For that purpose, changes in the scale of prototypes were needed to measure dynamic stresses properly. Furthermore, in the work presented by [35], a Darrieus tidal turbine was studied in wind and water tunnel. Wind experiments were used to study the starting and dynamic torque, and the suitability of different blade geometries. After that, the water tunnel was used to verify the dynamic torque value and to obtain the maximum tip speed ratio of the turbine under low flow conditions. Finally, in the studies carried out by [36] or [37] they made an accurate study of blockage effects but only considering those produce by wake phenomenon. Thus, it was possible to quantify the effect that the presence of the rotor produces on other turbines specially when they are arranged in arrays. However, none of these publications address the study of blockage conditions by testing the turbine under different fluids and focusing only on power parameters differences.

This article shows the analysis of the power stage of a vertical axis turbine (squirrel cage-Darrieus type) with straight blades manufactured by the help of additive technology. The power characterization study has been made in a wind tunnel located at the Polytechnic School of Engineering of Gijon (EPI) and in a water current flume settled in the Polytechnic School of Engineering of Mieres (EPM), both belonging to the University of Oviedo (Spain). Wind tests will obtain the behavior of the turbine at open-field conditions while water experiments will represent blockage conditions. Finally, both situations will be analyzed separately so the results will be contrasted.

2. Theoretical bases

The theoretical bases that describe the experimental tests at wind and water tunnels are distinct since the turbine is subject to the influence of two different fluids (air and water). However, the operation of the turbine is analogous in both cases, so the results could be compared thanks to the dimensionless characterization of the fluid movement, which is carried out by applying the Reynolds number. This dimensionless number,

Preprints (www.preprints.org) | NOT PEER-REVIEWED | Posted: 31 March 2021 doi:10.20944/preprints202103.0772.v1

which relates inertial and viscous forces, makes it possible the comparison between air and water since, after matching the expressions, the wind speed must be ten times greater than water velocity. Equalizing the Reynolds number of water and wind ($Re_{water} = Re_{wind}$) implies that $U_{water} \approx 10 \cdot U_{wind}$; being Re_{water} and Re_{wind} the number of Reynolds at water and wind respectively (dimensionless) and U_{water} and U_{wind} the current velocity of the water or the wind (m/s).

2.1. Wind bases

The experimentation of the turbine model in the wind tunnel is based on the application of the actuator disk theory. In these circumstances the flow is incompressible, homogeneous, stationary and the rotor has and infinite number of blades, actuating a uniform thrust in all of them. The wind velocity upstream the disk (U_{wind}) is reduced as it approaches to the turbine (U_2), reaching its minimum value once the fluid has passed through the rotor (U_3) due to wake effects [38]. Also, far away from the disk (upstream and downstream) the static pressure of the air is equal to the atmospheric pressure (P_{atm}) (Figure 3).

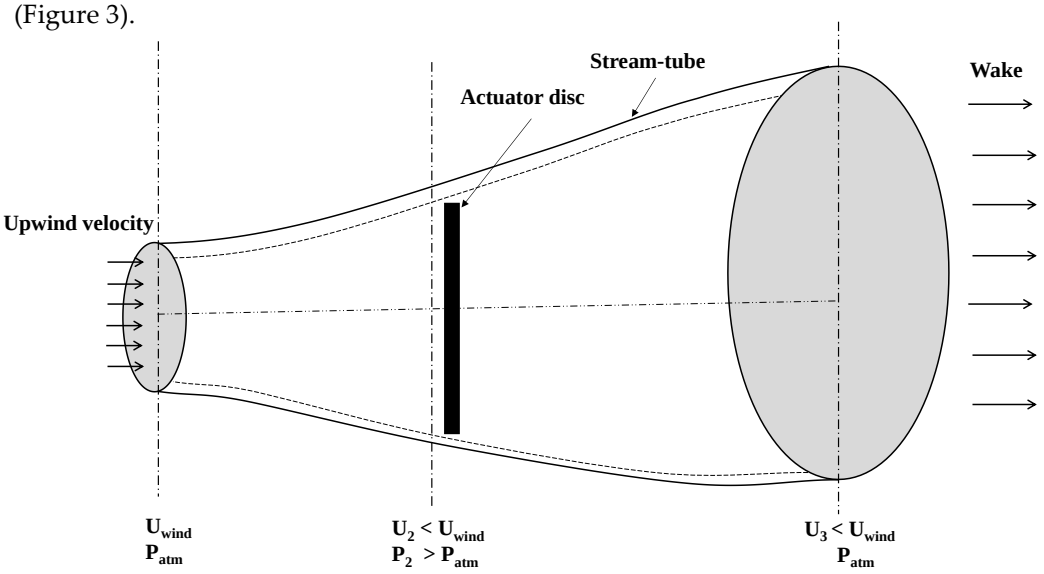

Figure 3. Actuator disk theory at wind tunnel.

Thus, as the water current approaches the rotor, there is a decrease in the wind speed since there is an extraction of energy by the turbine. Therefore, applying the linear momentum conservation equation to the considered control volume, the power extracted by the turbine depends on the wind density, the area swept by blades, the cubic expression of wind velocity and the power coefficient of the rotor. At maximum power conditions (MPP_{wind}), power coefficient is limited to 0.59, which corresponds with the Betz limit [39]

2.2. Water bases

The turbine model testing conditions inside the water channel follows the one-dimensional actuator disc model that porposed by Houlsby et al [40]. In this model, the rotor is working as a hydrokinetic turbine in conditions of uniform and subcritical flow due to the tunnel itself. More specifically, it is considered:

- There is a disk submerged in water and under blockage conditions produced by its presence in the channel.
- Two different zones with uniform flow are distinguished upstream and downstream of the disk. A mixing zone will also appear due to turbulence phenomena, being located just after the disk.
- Uniform flow zones have constant water velocity and subcritical conditions.

These conditions are produced in the hydrodynamic water tunnel using a water gate that is situated downstream the rotor. Furthermore, since the channel is made of glass

Preprints (www.preprints.org) | NOT PEER-REVIEWED | Posted: 31 March 2021 doi:10.20944/preprints202103.0772.v1

(low roughness) and the slope is practically horizontal, a constant velocity profile can be assumed (Figure 4).

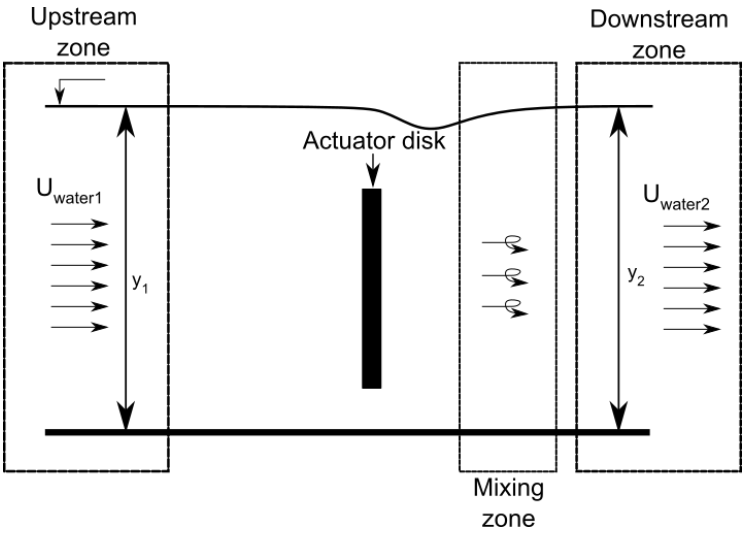

Figure 4. Actuator disk scheme at water tunnel.

It should be noted that the calculation of power in water turbines is carried out by applying the same expression as wind turbines but, due to the appearance of blockage conditions, the power coefficient is not limited so it can be higher than the Betz limit [19].

2.3. Testing Parameters

In both installations, the characterization of the power stage is carried out applying two dimensionless coefficients: tip speed ratio and power coefficient. Other parameters, such as the hydraulic and mechanical power, are also used. These are the equations used for their calculation:

$$TSR = \frac{\omega \cdot R}{U} \quad (1)$$

$$Cp = \frac{P_m}{P_t} \quad (2)$$

$$P_t = \frac{1}{2} \cdot \rho \cdot A_t \cdot U^3 \quad (3)$$

$$P_m = T \cdot \omega \quad (4)$$

Where TSR is the relation between the velocity at the tip of the blade and the fluid speed (dimensionless), ω is the rotational speed of the turbine (rad/s), R is the radius of the rotor (m), U is the fluid velocity (m/s), Cp is the power coefficient (dimensionless), P_m is the mechanical power (W), ρ is the fluid density (kg/m^3), A_t is the area swept by blades (m^2), U is the current velocity (m/s), P_t is the hydraulic power (W), and T is the torque measured by the torque meter (N).

Another hydrodynamic parameter of interest is blockage coefficient. It is defined as the ratio between the turbine area and the channel section.

$$BR = \frac{A_t}{A_c} = \frac{2 \cdot R \cdot h}{b \cdot y} \quad (5)$$

Where BR is the blockage ratio (dimensionless), A_c is the channel section (m^2), h is the height of the rotor (m), b is the width of the channel (m) and y is the height of the water sheet (m).

It is evident that wind and water tests will differ, and not only because two different fluids have been used. In this case, the tests made at the water tunnel are influenced by

Preprints (www.preprints.org) | NOT PEER-REVIEWED | Posted: 31 March 2021 doi:10.20944/preprints202103.0772.v1

blockage so it will be necessary to extrapolate the confined results to open-field conditions. For this, expressions must be applied to obtain the velocity at open-field conditions. Although there are many different formulations, in this case the corrections proposed by Gauvin et al [21] (Eq 6 and Eq.7) and Werle [25] (Eq 8) have been applied because they are suitable for low blockage coefficients [41].

$$\left(\frac{\bar{U}}{U_w}\right)^2 = 1 - m \cdot BR \quad (6)$$

$$m = 8{,}14 \cdot BR^2 - 7{,}309 \cdot B + 3{,}23 \quad (7)$$

$$\frac{U_w}{\bar{U}} = 1 - BR \quad (8)$$

$$TSR_F = TSR\left(\frac{U_w}{\bar{U}}\right) \quad (9)$$

$$Cp_F = Cp\left(\frac{U_w}{\bar{U}}\right)^3 \quad (10)$$

Where $\bar{U}$ is the water velocity at open-field conditions (m/s), m is an empirical factor (dimensionless), TSR_F is the tip speed ratio at open-field conditions (dimensionless) and Cp_F is the power coefficient at open-field conditions (dimensionless).

3. Materials and methods

3.1. Rotor description

The designed rotor has a height and radius of h=0.15 m and R=0.075 m respectively, with three blades spaced 120 degrees. A NACA-0015 standard profile with a chord of c=0.05 m has been used, so its solidity is of 2. This blade profile has been selected for its good behavior under low flow velocity conditions, far superior to asymmetric profiles [42]. Also, it has been decided to use a three-bladed rotor because there are more advantageous in terms of efficiency and cost [43]. Figure 5 shows (a) the geometric characteristics of the turbine and (b) the blade fabrication on a 3D printer.

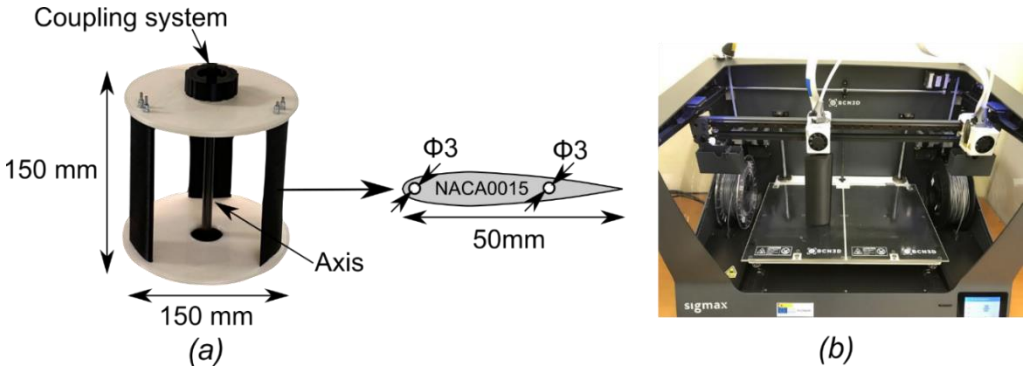

Figure 5. Geometric characteristics and fabrication process of the turbine model.

The turbine and its coupling system have been built using 3D additive manufacturing technology, being the Polylactic Acid (PA) the selected material. PA has an excellent behavior against dynamic stresses, has good durability working with water and is easily moldable so pieces can be adjusted to complex profiles like NACA 0015 [44]. For both experiments the shaft diameter has been of 10 mm.

3.2. Wind tunnel description

The wind tunnel has a total length of 13.75 m and a discharge section of 0.68 x 0.68 m, working like an open-air admission circuit and under subsonic conditions. In addition,

Preprints (www.preprints.org) | NOT PEER-REVIEWED | Posted: 31 March 2021 doi:10.20944/preprints202103.0772.v1

the discharge section where the different prototypes are located is also fully open, so there are no blockage conditions. The air movement is produced by an axial fan with a diameter of 1.2 m and a power of 30 kW, controlled by an electronic power inverter that allows maximum wind speeds up to 35.5 m/s. Figure 6 shows the characteristics of the wind tunnel, where (1) is the admission honeycomb panels, (2) is the axial fan, (3) is the diffuser section, (4) is the stilling chamber and (5) is the testing section.

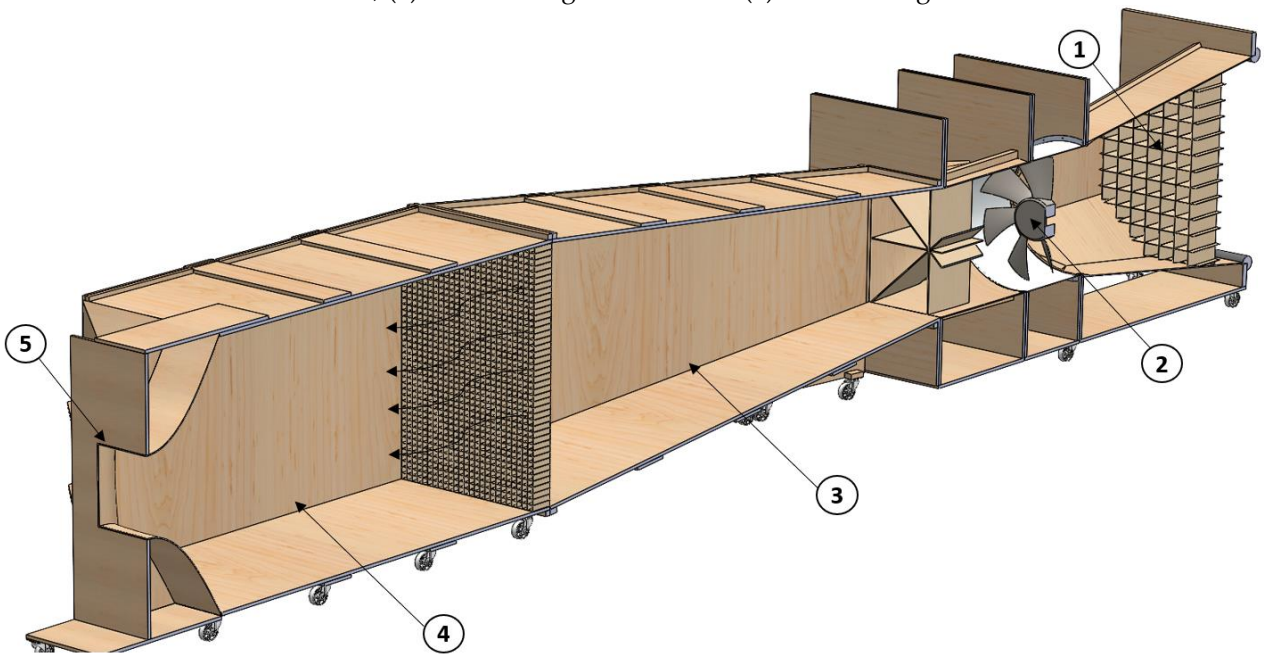

Figure 6. Wind tunnel configuration.

To reduce turbulent phenomena, the wind tunnel has a stilling chamber and honeycomb panels all along the facility. Also, the installation has different sensors that allow the parametrization of tests conditions. More specifically, Pitot tubes and differential and digital manometers are available, so wind speed and pressure are known.

The prototypes are tested in the channel using a portable aluminum structure where the rotor and measurement instruments are located. This structure allows the variation of the height and distance of the position of the prototype so test conditions can be easily changed. The rotational axis is coupled above and below by two high-performance radial bearings, being the rotor located between them. In the upper part, it is situated the torque meter and electric brake to carry out the wind power characterization tests of the turbine. Figure 7 shows in (a) the different devices used during a wind test and (b) the turbine at the testing section. (1) are the power supply devices, (2) is the tested turbine, (3) is the computer where all data is collected, (4) is the aluminum structure, (5) is the torque meter and (6) is the digital manometer.

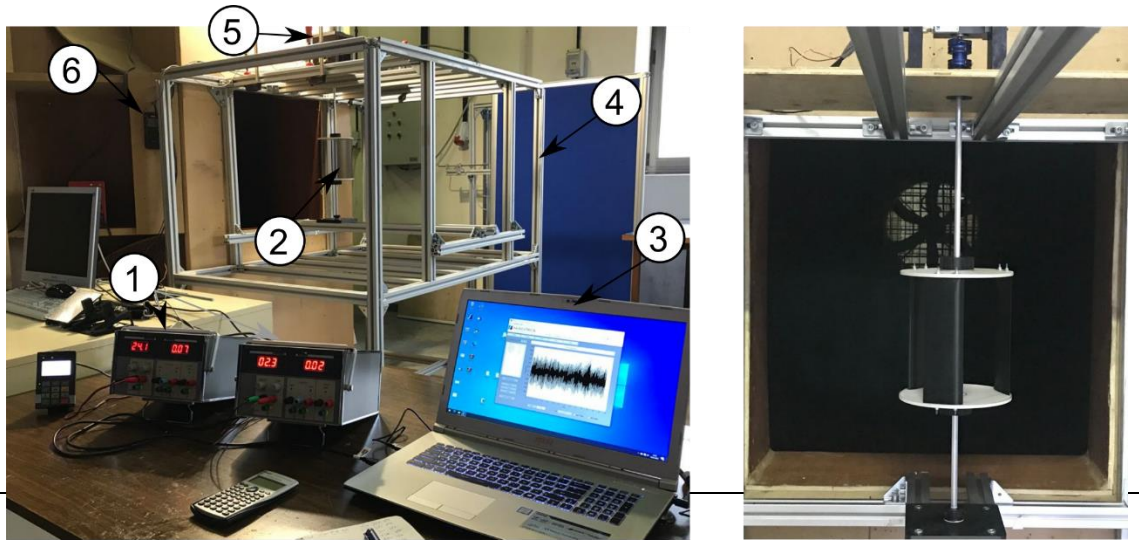

Preprints (www.preprints.org) | NOT PEER-REVIEWED | Posted: 31 March 2021 doi:10.20944/preprints202103.0772.v1

Figure 7. Turbine model at the wind tunnel.

3.3. Water tunnel description

The water current flume has a rectangular section with a length of 1.5 m, a height of 0.55 m and a wide of 0.3 m, being the floor and walls made of laminated glass allowing the recording of the tests. The flow movement is generated by a hydraulic pumping system with a total power of 30 kW that can move a maximum flow rate of 600 m^3/h. Both pumps are controlled by two electronic inverters through the variation of the electrical supply frequency. The whole system works as a close circuit, suctioning the water from a recirculation tank of 5 m^3 and driving it superiorly towards the hydraulic testing channel. At the end of the channel a metallic gate controlled by a gear system is installed to induce low-velocity hydrokinetic conditions. Figure 8 shows the description of the water tunnel, where (1) are the hydraulic pumps, (2) the electronic system, (3) the reassuring tank, (4) channel and rotor, (5) the water gate and (6) suction tank.

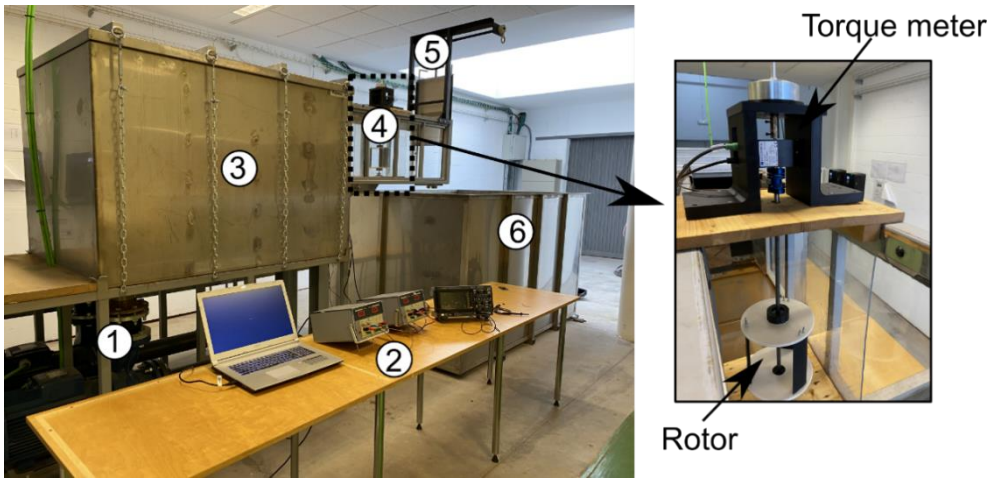

Figure 8. Water current flume including the turbine model.

To test the turbine, it has been designed and built a water-resistant methacrylate box. This structure has in its submerged part a waterproof radial bearing that allows the rotation of the axis in optimal conditions. In the upper part and out of the water current, a lid is available for the location of the torque meter and electric brake. It should be noted that this structure can be easily installed and removed due to the anchoring system based on slide clamps, so the different rotors can be quickly tested.

3.4. Testing procedure

To study the power stage of the described turbine, a high precision torque meter has been used together with an electromagnetic brake. This procedure has been used both in the wind tunnel and in the water current flume. On the one hand, the torque meter has a rated torque of 0.5 Nm and a maximum torque measurement of 1 Nm, being calibrated according to the standards of the Swiss Federal Institute of Metrology (METAS). This device allows measurements of torque, rotational speeds, and relative position of the blades with data-taking frequencies up to 80 data per second, achieving a good sampling spectrum. All collected data is sent to a database for further processing. On the other hand, the variation of the braking force is controlled by varying voltage using a power supply device.

Preprints (www.preprints.org) | NOT PEER-REVIEWED | Posted: 31 March 2021 doi:10.20944/preprints202103.0772.v1

The characterization procedure starts with an initial measurement where no braking force is applied, so the rotor has its maximum rotational speed but without power generation. This step is called "no-load condition". Subsequently, the resistive torque of the electric brake is sequentially changed through voltage variations at power supply device, obtaining different extracted powers and rotational speeds for each one. That is, for each voltage, a TSR (λ) and power value will be captured. The procedure continues until the rotor stops its rotation (see

Figure **9**).

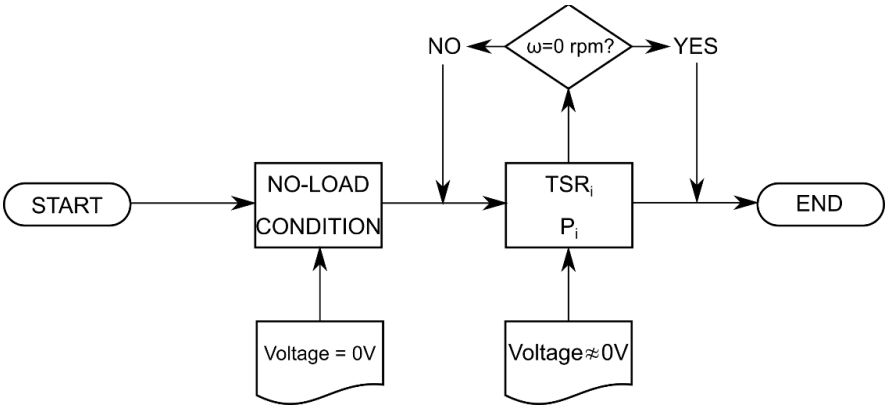

Figure 9. Experimental test procedure.

4. Results

The turbine has been tested in the wind tunnel under real open-field conditions which following the actuator disc assumptions that have been listed before. It has been tested at four different wind velocities varying from 7 to 10 m/s. in fact, this model has been tested for flow velocities higher than 10 m/s reaching 20 m/s and proved stability, reliability, and durability, but it should be born in mind that these higher velocities are somewhat rare, particularly in the urban environment which make our point of investigation is focused on real world performance, not the artificial one.

During the different tests, continuous measurements of parameters, such as torque and angular velocity, were carried out. Thus, it was possible to check if the turbine reached stability before starting the power test in each point, minimizing discontinuities. As after loading the turbine rotor, it was desirable to wait and watch the rotational speed variation of the turbine rotor before recording results to assure that the turbine is working under stable conditions. Figure 10 illustrates the stability condition during one of the proposed tests.

Preprints (www.preprints.org) | NOT PEER-REVIEWED | Posted: 31 March 2021 doi:10.20944/preprints202103.0772.v1

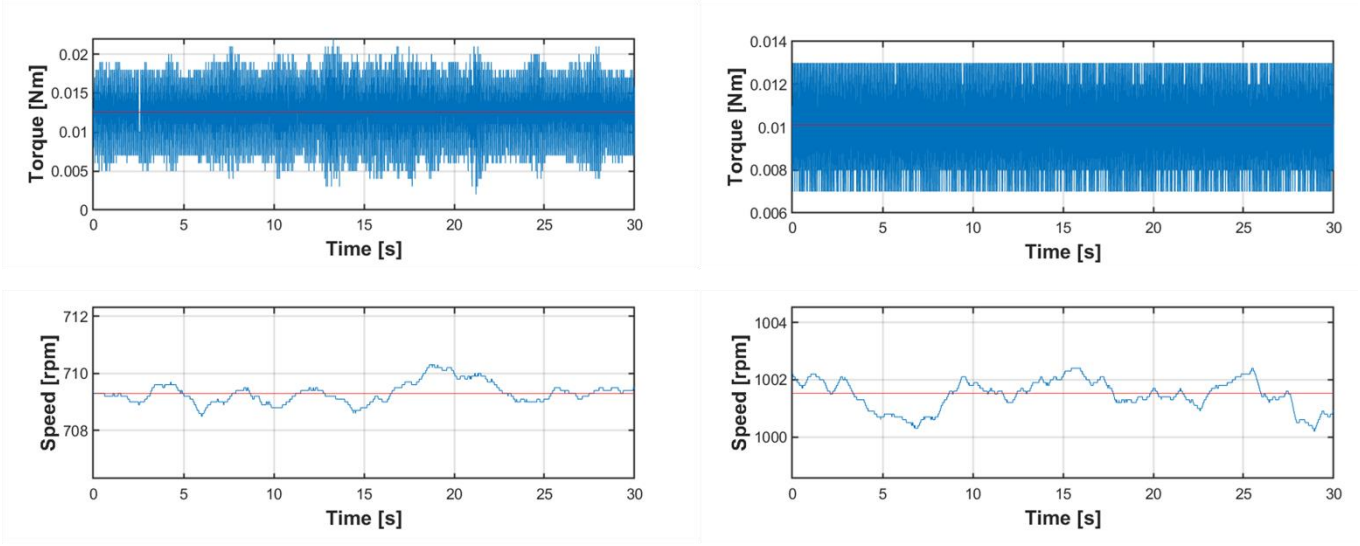

Figure 10. Stability conditions for low and high rotational speeds test conditions at wind speed of 8 m/s.

The variation of the power output with the rotational speed of the turbine rotor for different upstream wind velocities are shown in Figure 11. All tested speeds show the same tendency, as by loading the turbine rotor, the rotational speed decreased, and the output power increased dramatically till reaching the maximum power point. After that, the power output started to decline till reaching the point where the turbine stops and not able to produce more power. In fact, for high flow velocities, the power curve leans to complete after reaching the *MPP*, but for low velocities the power curve is nearly reached the *MPP* and does not complete. This due to the power to friction ratio, as for high flow velocity, the turbine model is able to produce power to overcome the friction and pass the *MPP*, on the other hand, for low velocities the rotor is not able to pass this point and to characterize this part of the power curve an active control system is needed.

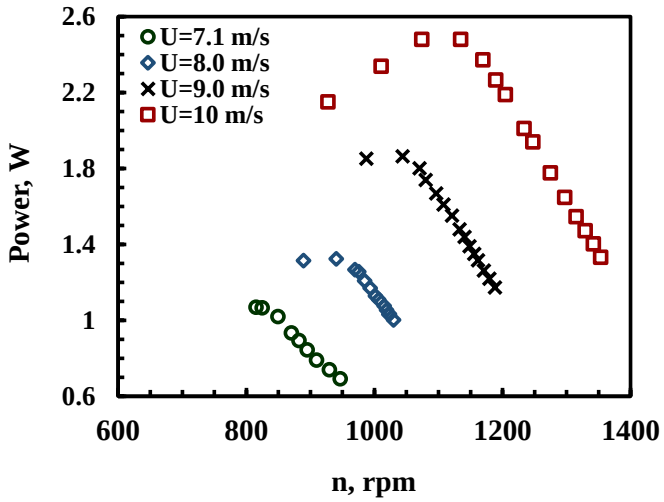

Figure 11. Wind tunnel power curves at different upstream velocities.

By tracking the maximum power point *MPP* variation with the upstream wind velocity (Figure 12) it was found that the maximum power increases nearly with the cube of the upstream wind velocity, as Eq 3 indicates, to reach its maximum value of 2.5 W at wind velocity of 10 m/s.

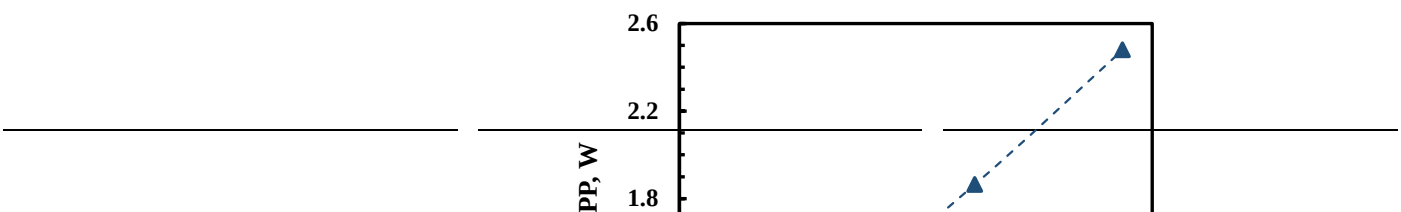

Preprints (www.preprints.org) | NOT PEER-REVIEWED | Posted: 31 March 2021 doi:10.20944/preprints202103.0772.v1

Figure 12. Maximum power point variation with wind velocities.

The turbine model characteristic curve inside the wind tunnel is shown in Figure 13. The rotor is observed to work in a stable Cp range of approximately 0.13, being this maximum point reached at a λ of 1.1. Additionally, all curves seem to be identical which mean the turbine rotor works properly under open-field conditions without existing of other factor like blockage. In fact, the value of tip speed ratio is considered small compared with other turbines of the same model, this is returns to the high solidity value that was selected in the proposed model to allow a self-starting under low flow velocities.

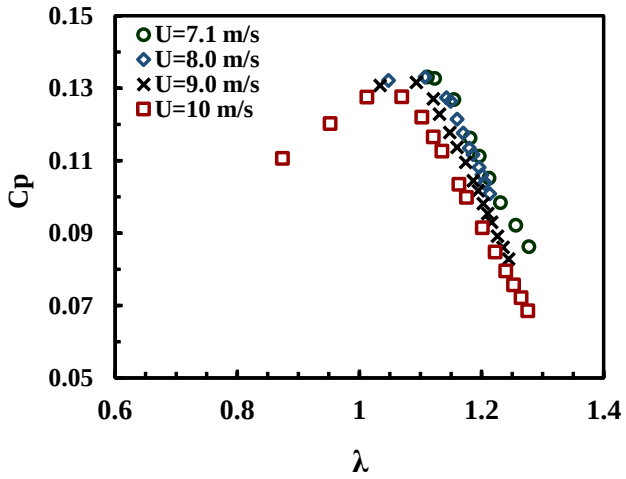

Figure 13. Characteristic curve for the turbine model at different wind velocities.

To study the effects of blockage conditions and their correction to open-field behavior, the turbine has been tested in the open-surface water channel. Four tests have been carried out for similar velocities and different blockage values ranging from 0.2 to 0.35. Figure 14.a. shows the variation of the characteristic curves with the blockage. Different curves have been obtained for the same rotor while for wind tests only one curve was drawn. This is due to the existence of flow blockage conditions that affect the rotor performance, by increasing the blockage value the performance curves are shifted to higher values of tip speed ratios and power coefficients. It is a result of the flow acceleration around the turbine rotor while the blockage increased. As shown in Figure 14. b, with a turbine rotor blockage value of 6.8% inside the wind tunnel, which is considered as an open field condition, the maximum power coefficient value is of 0.13. By increasing the blockage value from 6.8% to 35%, the maximum power coefficient increased to reach its maximum value of 0.97.

Preprints (www.preprints.org) | NOT PEER-REVIEWED | Posted: 31 March 2021 doi:10.20944/preprints202103.0772.v1

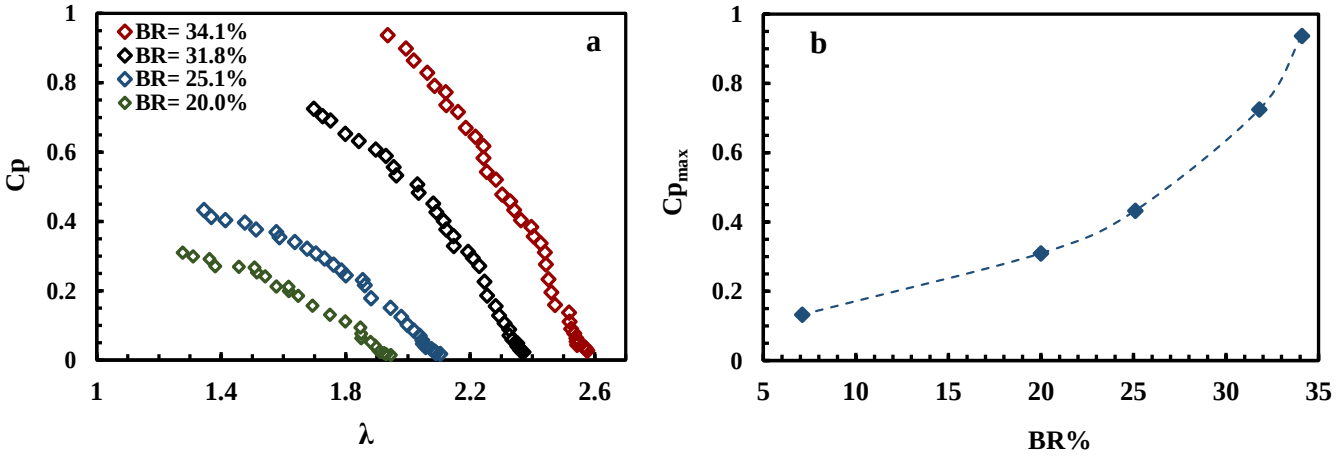

Figure 14. (a) Characteristic curves at different water blockage values, (b) Variation of Cp_{max} with Blockage ratio.

The extrapolation of blockage to open-field conditions have been made using the flow velocity of 0.71 m/s with a BR of 0.2. Under these conditions, the rotor works Reynolds number of 2.5 10^4 approximately, so results between wind and water can be compared. After applying the formulation of Gauvin et al and Werle, the $\bar{U}$ of 0.92 m/s and 0.875 m/s have been obtained, respectively. Figure 15 shows a comparison between results obtained at wind tunnel, confined water channel and those corrected with the blockage correction formulation.

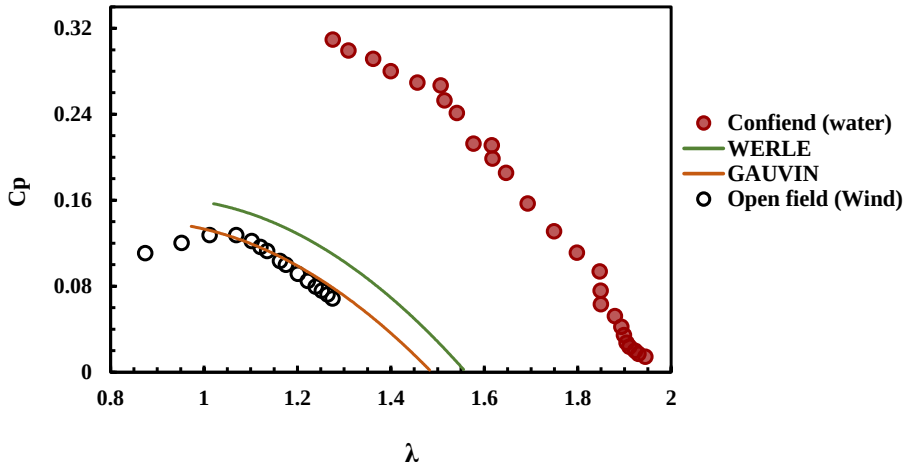

Figure 15. Cp vs tip speed ratio for wind and water tunnel (Re = 2.5 10^4 approximately).

The peak power coefficient for the confined flow condition reached a value of 0.31 which is 1.5 times higher than the peak one for the experimental open field condition. Actually, the corrected results including (Werle and Gauvin) are quite similar to the results obtained from wind tunnel tests, however Werle formulations gives results slightly higher reaching Cp value nearly of 0.16 which is higher than the experimental one by about 0.13. The tip speed ratio that corresponds to the maximum power coefficient values coincide in both cases and are greater than 1.

5. Conclusions

The combined use of hydrokinetic and wind turbines farms is considered one of the modern developments in the energy sector for urban communities and smart cities which will be able to provide energy to nearby consumption points. The use of vertical-axis crossflow turbine based on Darrieus designs is considered one of the best options for rural and urban areas with the installation of permanent magnet generators and the development of new electronic power stage control systems.

A turbine has been tested in the wind tunnel under real open-field conditions at four wind velocities varying from 7 to 10 m/s. Stability conditions in terms of rotational speed and output torque which reflects the quality of the extracted results were showed. Power curves have been obtained for each tested wind velocity, also the maximum power point *MPP* increases nearly with the cube of the upstream wind velocity, to reach its maximum value of 2.5 W at wind velocity of 10 m/s.

Characteristic curves for the rotor inside the wind tunnel at different upstream wind velocities seem to be identical which mean the turbine rotor works properly under open-field conditions without existing of any other factors like blockage.

The turbine has been tested at open-surface water channel for different blockage values ranging from 0.2 to 0.35. Different characteristic curves have been obtained for the same rotor due to the existence of different flow blockage conditions. Increasing the blockage value shifts the performance curves to higher values of tip speed ratios and power coefficients due to the flow acceleration around the turbine rotor while the blockage increased. The turbine has a maximum power coefficient of 0.13 for blockage ration of 6.8% (inside wind tunnel), increasing the blockage value from 6.8% to 35% rises the maximum power coefficient increased to reach its maximum value of 0.97.

For a blockage of 20% the peak power coefficient for the confined flow condition reached a value of 0.31 which is 1.5 times higher than the peak one for the experimental open field condition at the same Reynolds number. In addition, two blockage correction formulations (Werle and Gauvin) are applied to the water channel tests, which gave values quite similar to the results obtained from wind tunnel tests, however Werle formulations gives results slightly higher, reaching Cp value nearly of 0.16, which is higher than the experimental one by about 23.1%.

Acknowledgments: The authors would like to express their gratitude to the Institute of Economic Development of the Principality of Asturias (Spain), the Egyptian Cultural Affairs and Missions Sector (the Egyptian Ministry of Higher Education and Scientific Research) for their financial support and to the International Association for Hydro-Environment Engineering and Research (IAHR) for the opportunity provided at the VI IAHR 2020 Europe Congress of Poland in which a small preview of the research was presented.

References

[1] C. Espejo-Marín and A. E. Aparicio-Guerrero, "La Producción de Electricidad con Energía Solar Fotovoltaica en España en el Siglo XXI.," *Rev. Estud. Andaluces*, no. 39, pp. 66–93, 2020, doi: 10.12795/rea.2020.i39.04.

[2] H. Díaz and C. Guedes Soares, "Review of the current status, technology and future trends of offshore wind farms," *Ocean Engineering*, vol. 209. Elsevier Ltd, p. 107381, Aug. 01, 2020, doi: 10.1016/j.oceaneng.2020.107381.

[3] IEA, "Energy Technology Perspectives 2020," 2020. doi: 10.1787/ab43a9a5-en.

[4] REN21, "Renewables 2020 Global Status Report: Nota de prensa," 2020. [Online]. Available: https://www.ren21.net/wp-content/uploads/2019/05/GSR_2020_Press_Release_ES.pdf.

[5] IRENA, "Global Renewables Outlook: Energy transformation 2050," 2020. [Online]. Available: https://www.irena.org/publications/2020/Apr/Global-Renewables-Outlook-2020.

[6] IDAE, "Plan de Energías Renovables 2011- 2020.," 2011. https://www.idae.es/tecnologias/energias-renovables/plan-de-energias-renovables-2011-2020 (accessed Jan. 05, 2021).

[7] F. Oreste, M. G. Vittorio, and P. Francesco, "Numerical assessment of the vulnerability to impact erosion of a pump as turbine in a water supply system," *J. Hydroinformatics*, vol. 22, no. 4, pp. 691–712, Jul. 2020, doi: 10.2166/hydro.2020.140.

[8] G. Bogdan Gherman, I. Mălăel, B. George Gherman, and I. Porumbel, "Increase the Smart Cities Development by Using an Innovative Design for Vertical Axis Wind Turbine," pp. 506–0513, doi: 10.2507/27th.daaam.proceedings.076.

[9] E. Alvarez Alvarez, M. Rico-Secades, E. L. Corominas, N. Huerta-Medina, and J. Soler Guitart, "Design and control strategies for a modular hydroKinetic smart grid," *Int. J. Electr. Power Energy Syst.*, vol. 95, pp. 137–145, Feb. 2018, doi: 10.1016/j.ijepes.2017.08.019.

[10] Z. Yuan, W. Wang, and X. Fan, "Back propagation neural network clustering architecture for stability enhancement and harmonic suppression in wind turbines for smart cities," *Comput. Electr. Eng.*, vol. 74, pp. 105–116, Mar. 2019, doi: 10.1016/j.compeleceng.2019.01.006.

[11] S. Mohammadi, M. Hassanalian, H. Arionfard, and S. Bakhtiyarov, "Optimal design of hydrokinetic turbine for low-speed water flow in Golden Gate Strait," *Renew. Energy*, vol. 150, pp. 147–155, May 2020, doi: 10.1016/j.renene.2019.12.142.

[12] J. H. Lee, S. Park, D. H. Kim, S. H. Rhee, and M. C. Kim, "Computational methods for performance analysis of horizontal axis tidal stream turbines," *Appl. Energy*, vol. 98, pp. 512–523, 2012, doi: 10.1016/j.apenergy.2012.04.018.

[13] C. A. Consul, R. H. J. Willden, E. Ferrer, and M. D. Mcculloch, "Influence of Solidity on the Performance of a Cross-Flow Turbine," pp. 484–493, 2009.

[14] M. J. Khan, G. Bhuyan, M. T. Iqbal, and J. E. Quaicoe, "Hydrokinetic energy conversion systems and assessment of horizontal and vertical axis turbines for river and tidal applications: A technology status review," *Appl. Energy*, vol. 86, no. 10, pp. 1823–1835, 2009, doi: 10.1016/j.apenergy.2009.02.017.

[15] S. Kaprawi, D. Santoso, and R. Sipahutar, "Performance of combined water turbine darrieus-savonius with two stage savonius buckets and single deflector," *International Journal of Renewable Energy Research*, 2015. https://repository.unsri.ac.id/7412/ (accessed Mar. 06, 2021).

[16] A. E. Benchikh Le Hocine, R. W. Jay Lacey, and S. Poncet, "Multiphase modeling of the free surface flow through a Darrieus horizontal axis shallow-water turbine," *Renew. Energy*, vol. 143, pp. 1890–1901, Dec. 2019, doi: 10.1016/j.renene.2019.06.010.

[17] F. Balduzzi *et al.*, "Understanding the Aerodynamic Behavior and Energy Conversion Capability of Small Darrieus Vertical Axis Wind Turbines in Turbulent Flows," *Energies*, vol. 13, no. 11, p. 2936, Jun. 2020, doi: 10.3390/en13112936.

[18] M. Sinagra, V. Sammartano, C. Aricò, A. Collura, and T. Tucciarelli, "Cross-Flow turbine design for variable operating conditions," in *Procedia Engineering*, Jan. 2014, vol. 70, pp. 1539–1548, doi: 10.1016/j.proeng.2014.02.170.

[19] R. Espina-Valdés, A. Fernández-Jiménez, J. Fernández Francos, E. Blanco Marigorta, and E. Álvarez-Álvarez, "Small cross-flow turbine:Design and testing in high blockage conditions," *Energy Convers. Manag.*, vol. 213, p. 112863, Jun. 2020, doi: 10.1016/j.enconman.2020.112863.

[20] H. Glauert, "Wind Tunnel Interference on Wings, Bodies and Airscrews," *Aeronaut. Res. Comm.*, no. 1566, pp. 1–52, 1933.

[21] O. Gauvin-Tremblay and G. Dumas, "Two-way interaction between river and deployed cross-flow hydrokinetic turbines," *J. Renew. Sustain. Energy*, vol. 12, no. 3, p. 034501, May 2020, doi: 10.1063/5.0004492.

[22] J. Schluntz and R. Willden, "The effect of blockage on tidal turbine rotor design and performance," vol. 23, no. 3, p. 2019, 2015.

[23] R. Vennell, "Exceeding the Betz limit with tidal turbines," *Renew. Energy*, vol. 55, pp. 277–285, 2013, doi: 10.1016/j.renene.2012.12.016.

[24] A. S. Bahaj, A. F. Molland, J. R. Chaplin, and W. M. J. Batten, "Power and thrust measurements of marine current turbines under various hydrodynamic flow conditions in a cavitation tunnel and a towing tank," *Renew. Energy*, vol. 32, no. 3, pp. 407–426, 2007, doi: 10.1016/j.renene.2006.01.012.

[25] M. J. Werle, "Wind turbine wall-blockage performance corrections," *J. Propuls. Power*, vol. 26, no. 6, pp. 1317–1321, May 2010, doi: 10.2514/1.44602.

[26] H. C. Soerensen and A. Weinstein, "Ocean Energy: Position paper for IPCC," 2009.

[27] A. H. Birjandi, E. L. Bibeau, V. Chatoorgoon, and A. Kumar, "Power measurement of hydrokinetic turbines with free-surface and blockage effect," *Ocean Eng.*, vol. 69, pp. 9–17, 2013, doi: 10.1016/j.oceaneng.2013.05.023.

[28] P. Bachant and M. Wosnik, "Performance measurements of cylindrical- and spherical-helical cross-flow marine hydrokinetic turbines, with estimates of exergy efficiency," *Renew. Energy*, vol. 74, pp. 318–325, 2015, doi: 10.1016/j.renene.2014.07.049.

[29] N. Kolekar, A. Vinod, and A. Banerjee, "On Blockage E ff ects for a Tidal Turbine in Free Surface Proximity," 2019.

[30] C. A. Consul, R. H. J. Willden, and S. C. McIntosh, "Blockage effects on the hydrodynamic performance of a marine cross-flow turbine," *Philos. Trans. R. Soc. A Math. Phys. Eng. Sci.*, vol. 371, no. 1985, 2013, doi: 10.1098/rsta.2012.0299.

[31] G. Brochier, P. Fraunie, C. Beguier, and I. Paraschivoiu, "Water channel experiments of dynamic stall on darrieus wind turbine blades," *J. Propuls. Power*, vol. 2, no. 5, pp. 445–449, May 1986, doi: 10.2514/3.22927.

[32] N. Fujisawa and S. Shibuya, "Observations of dynamic stall on turbine blades," *J. Wind Eng. Ind. Aerodyn.*, vol. 89, no. 2, pp. 201–214, Feb. 2001, doi: 10.1016/S0167-6105(00)00062-3.

[33] M. Sherry, J. Sheridan, and D. Lo Jacono, "Horizontal axis wind turbine tip and root vortex measurements," 2010.

[34] G. V. Iungo, F. Viola, S. Camarri, F. Porté-Agel, and F. Gallaire, "Linear stability analysis of wind turbine wakes performed on wind tunnel measurements," *J. Fluid Mech.*, vol. 737, pp. 499–526, Dec. 2013, doi: 10.1017/jfm.2013.569.

[35] K. Hiraki, R. Wakita, and M. Inoue, "Improvement of straight-bladed vertical-axis water turbine for tidal current power generation," *Proc. 9th ISOPE Pacific/Asia Offshore Mech. Symp. PACOMS-2010*, pp. 169–174, 2010.

[36] M. Shahsavarifard, E. L. Bibeau, and V. Chatoorgoon, "Effect of shroud on the performance of horizontal axis hydrokinetic turbines," *Ocean Eng.*, vol. 96, pp. 215–225, Mar. 2015, doi: 10.1016/j.oceaneng.2014.12.006.

[37] H. Jeong, S. Lee, and S. D. Kwon, "Blockage corrections for wind tunnel tests conducted on a Darrieus wind turbine," *J. Wind Eng. Ind. Aerodyn.*, vol. 179, pp. 229–239, Aug. 2018, doi: 10.1016/j.jweia.2018.06.002.

[38] S. N. Ruiz, "Aerogeneradores de media potencia "," *CIEMAT*, 2020.

[39] T. Nishino and R. H. J. Willden, "The efficiency of an array of tidal turbines partially blocking a wide channel," *J. Fluid Mech.*, vol. 708, no. May 2014, pp. 596–606, 2012, doi: 10.1017/jfm.2012.349.

[40] S. Draper, G. T. Houlsby, M. L. G. Oldfield, and A. G. L. Borthwick, "Modelling tidal energy extraction in a depth-averaged coastal domain," *IET Renew. Power Gener.*, vol. 4, no. 6, pp. 545–554, 2010, doi: 10.1049/iet-rpg.2009.0196.

[41] E. Álvarez-Álvarez, M. Rico-Secades, A. Fernández-Jiménez, R. Espina-Valdés, E. L. Corominas, and A. J. Calleja-Rodríguez, "Hydrodynamic water tunnel for characterization of hydrokinetic microturbines designs," *Clean Technol. Environ. Policy*, vol. 22, no. 9, pp. 1843–1854, Nov. 2020, doi: 10.1007/s10098-020-01924-w.

[42] V. Patel, T. I. Eldho, and S. V. Prabhu, "Experimental investigations on Darrieus straight blade turbine for tidal current application and parametric optimization for hydro farm arrangement," *Int. J. Mar. Energy*, vol. 17, pp. 110–135, 2017, doi: 10.1016/j.ijome.2017.01.007.

[43] T. Burton, N. Jenkins, D. Sharpe, and E. Bossanyi, *Wind Energy Handbook*. Chichester, UK: John Wiley & Sons, Ltd, 2011.

[44] F. Calignano, M. Lorusso, I. Roppolo, and P. Minetola, "Investigation of the Mechanical Properties of a Carbon Fibre-Reinforced Nylon Filament for 3D Printing," *Machines*, vol. 8, no. 3, p. 52, Sep. 2020, doi: 10.3390/machines8030052.